Analytical and numerical instability analysis of functionally graded low-carbon steel

K. Amirian [1], Z. Abbasi [2], R. Ebrahimi *[3]

[1, 3] Department of Materials Science and Engineering, School of Engineering, Shiraz University, Shiraz, Iran
[2] Physics of Nanostructured Materials, Dynamics of Condensed Systems, Faculty of Physics, Vienna University, Vienna, Austria

Abstract

The instability point of a material is one of the most important factors when choosing a material, as it could be a good representation of its formability. In this study, the instability of functionally graded materials (FGM) was investigated. An algorithm is proposed for predicting the instability of functionally graded low-carbon steel with gradient work hardening exponent (n) and strength coefficient (K). The investigated work hardening exponent and strength coefficient of the FGM vary through the cross-section as a function of radius. Numerical methods like the Simpson rule of integration were utilized to solve the equations. The mathematical and experimental results are compared, and it can be seen that the algorithm has a reliable consistency with the experimental results. The presented analysis shows that the instability of the functionally graded low-carbon steel can be predicted using the calculation of the average strain hardening exponent. The calculated average work hardening exponent ($\bar{n}$) was 0.1095 and 0.1657 for the 550 °C and 650 °C annealed samples, respectively. The instability of more complicated FGMs can be predicted with the present algorithm.

Keywords: FGM, Low-carbon steel, work hardening exponent, Strength coefficient, Gradient grain size.

1. Introduction

Improvements in material quality are made every day thanks to research and development efforts, but there is still no way to ensure that widely used materials like pure metals, alloys, and standard composites always maintain the essential characteristics required by many different types of machinery and equipment [1,2]. Limitations in using traditional homogenous materials necessitated the creation of new materials with contrasting properties and a graded structure to fulfill the needs of applications caused by technological and industrial progress [3]. This resulted in the development of a new class of materials known as functionally graded materials (FGM).

In recent years, FGMs have gained considerable attention in many engineering applications. FGMs are considered potential structural materials for future high-speed spacecraft, biomedical implants, power generation, and nuclear industries [4]. The phrase "functionally graded material" was originally used in Japan in 1984 to describe the development and use of thermal barrier materials [5]. Conventional FGMs are a novel class of composites with no internal borders or interfacial stress concentrations, resulting in a continuous distribution of microstructure and mechanical characteristics [6]. These materials are also known as sophisticated engineered materials in which the properties are customized and vary smoothly and continuously from one surface to the other [7,8]. In an FGM, the composition and structure gradually

**Corresponding author*
Email: ebrahimy@shirazu.ac.ir
Address: Department of Materials Science and Engineering, School of Engineering, Shiraz University, Shiraz, Iran
1. B.S. student
2. Research Assistant
3. Professor

change over volume, providing continuous graded macroscopic properties [9]. The gradual changes should be at least in one direction, which can be in the composition of the material or even its microstructure like grain size or porosity, resulting in at least one functional change in properties, such as hardness, wear resistance, corrosion resistivity, thermal conductivity, or specific heat [9,10].

Because of this smooth, continuous, and gradual transition in mechanical characteristics of FGM, they are better and more attractive than traditional composite materials, which have limitations such as sudden shifts along the composite borders [11]. Interest in FGMs has skyrocketed due to the vast opportunities it presents for producing individualized products well suited for many high-tech sectors. So, there has been a meteoric rise in the previous two decades in the number of scholarly articles covering this topic [11]. The concept of FGM was first developed for heat-resistant materials. Still, these materials have since been utilized to manage deformation, pressure, wear, and corrosion and to lessen stress concentration through a gradual transition across all product dimensions [12]. For example, metal cutting tools may benefit from having a composition gradient designed for the length of use and resistance to wear [13]. Likewise, the longevity and stability of dental implants may be enhanced by adjusting composition gradients and gradient thickness [14]. In the marine industry, FGMs may be utilized to create things like composite pipe systems, sonar domes, and propeller shafts. Due to their high price, FGMs are still not widely employed in the automotive industry. However, FGMs may be used in the production of a variety of car parts, including the combustion chamber, leaf spring, diesel engine piston, etc. [15].

By applying the many possibilities inherent in the FGM concept, it is anticipated that materials will be improved, and new functions for them and new processing solutions will be developed to simplify the process of making them [13]. Several studies have been performed to analyze the behavior of functionally graded plates and shells. Qiu et al.[16] developed an equation to determine the work hardening exponent for ultrafine grain low-carbon steels, resulting in a change in the work hardening exponent (n). Similarly, Sinclair et al. [17] investigated the relationship between work hardening and grain size. Wang et al. [18] used pre-torsion deformation and half an hour of 550 °C - 700 °C thermal annealing to create diverse low-carbon steel samples with grain size distribution.

One of the most important considerations when choosing a material for a particular application is its formability, or how easily it can be shaped while maintaining the desired quality. The capacity to undergo plastic deformation is what this term alludes to [19]. From a metallurgical standpoint, a metal's formability is determined by its elongation, the total amount of strain observed during tensile testing, which is the degree of deformation feasible during a metal-forming process without generating an undesirable condition, such as necking [20]. According to Considère, necking occurs as a consequence of instability in tensile deformation when the sample's cross-sectional area decreases at a faster rate than the material strain hardens, which for homogenous materials Considère approved that instability occurs at true strain equal to the work hardening exponent of the material obtained from the Hollomon equation [19].

Furthermore, in most cases, physical testing, such as tensile or microhardness testing, is required to measure the mechanical properties of materials such as functionally graded ones. This has some problems associated with it. Firstly, when doing most mechanical, the physical sample must be destroyed, which causes extra expenses. Secondly, the only place these tests can provide accurate readings is the exact spot where they are carried out. Because of this, numerical simulation and computation come into play, with which you are not bounded by the limitations of traditional tests.

In this study, an algorithm is driven to examine the instability of materials with grain size distribution along their radius, following a change in work hardening exponent (n) and strength coefficient (K). To confirm our work, we utilized our algorithm on Wang's samples and compared our results. Similar to Qiu et al. [16] the relationship between radius and work hardening exponent was found for the low-carbon steel samples with annealing temperatures of 550 °C and 650 °C. The relation between strength coefficient and radius was also found using the microhardness given for the samples; therefore, the technique was applied to model the low carbon steel specimens using the n and K grain size relations.

2. Mathematical procedure

The presented algorithm originated from the expression of force as stress integration on the area where the force is applied. As the considered material is functionally graded, its flow stress will vary with its location (r). Additionally, each point of material during deformation is susceptible to metallurgical changes, and therefore its flow stress will vary over time. Thus, the flow stress can be written as a function of both radius and time as follow:

$$F = \int_0^R \sigma(r,t)dA \qquad \text{Eq. (1)}$$

Where R is the radius of the specimen during deformation. The above equation is also valid for homogenous materials, with the main difference being that the stress is not a function of radius, as it is for the graded one. Furthermore, volume constancy can be used to understand R and the amount of strain as a function of time, as shown in Eqs. (2, 3).

$$R = \frac{R_0}{\sqrt{1 + t\frac{v}{L_0}}} \qquad \text{Eq. (2)}$$

$$\varepsilon = \ln(1 + t\frac{v}{L_0}) \qquad \text{Eq. (3)}$$

Where R_0 is the initial radius of the tensile test specimen, v is the crosshead speed, and L_0 is the initial length of the sample. Moreover, one of the best methods to approximate true stress-true strain curves is the Hollomon equation, as seen in Eq. (4).

$$\sigma = K\varepsilon^n \qquad \text{Eq. (4)}$$

Where, as understood, n is the work-hardening exponent, and K is the strength coefficient. For a homogeneous material, both variables are considered constant; however, for a functionally graded material, they can change through cross-section and be a function of radius. Accordingly, with the consideration of the Holloman equation and Eqs. (2-4), Eq. (1) can be rewritten as follow:

$$F = \int_0^{\sqrt{1+t\frac{v}{L_0}}R_0} K(r)(\ln(1 + t\frac{v}{L_0}))^{n(r)} 2\pi r dr \qquad \text{Eq. (5)}$$

The numerical computation of the algorithm is based on Eq. (5) and Simpson's integration approach. The algorithm was evaluated on a homogeneous material with the assumption that n and K are constant values before being used for an FGM. For instance, Fig. 1 was plotted using Eq. (5) in the case of a homogenous material with n = 0.3 and K = 100 MPa. The true strain at the maximum force is 0.296, which is very close to what was expected from the Considère criterion [19], that for a homogenous material, necking occurs at a true strain equal to the strain-hardening exponent, which in this case is 0.3. The engineering stress-engineering strain graph shown in Fig. 2 and the true stress-true strain curve presented in Fig. 3 were obtained from the force-displacement data illustrated in Fig. 1 using the classical relationship.

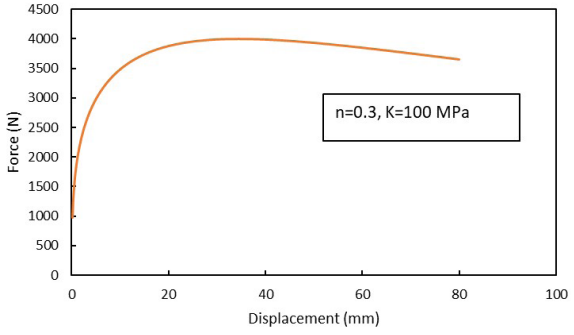

Fig. 1. The numerical force-displacement plot for a homogeneous material with n=0.3 and K=100 MPa.

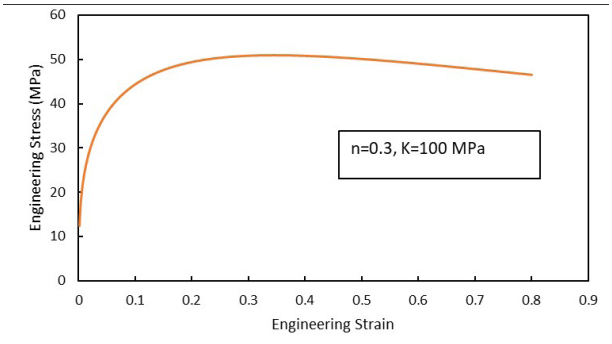

Fig. 2. The numerical engineering stress vs. engineering strain plot for a homogeneous material with n=0.3 and K=100 MPa.

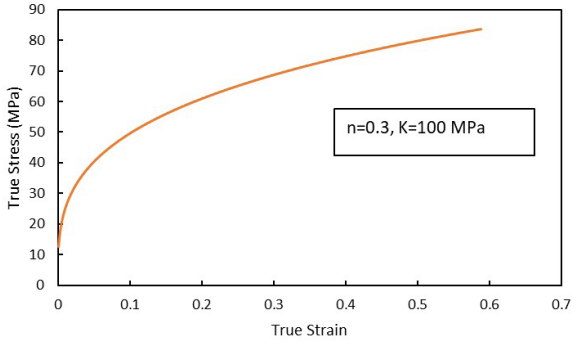

Fig. 3. The numerical and true stress-true strain plot for a homogeneous material with n=0.3 and K=100 MPa.

After the method has been validated for a homogeneous material, it can be applied to functionally graded materials. The data of functionally graded samples that this study was conducted on were adapted from Wang's study [18], in which he annealed the low-carbon steel dog bone samples with gauge dimensions of 5 mm diameter and 70 mm length at 550 °C and 650 °C after utilizing a pre-torsion test. His experiment led to the samples having grain size distributions and microhardness distributions with respect to the radius, as shown in Fig. 4 and Fig. 5, respectively. Moreover, in order to determine the distribution of n and K with respect to position using the indicated radius-to-grain-size relationships from Fig. 4, a similar work to Qui's experiment was utilized. Qui's investigation established Eq. (6) for relating grain size to the work hardening exponent in low-carbon steel.

$$n = 0.307 - 0.439D^{-\frac{1}{2}} \text{ (Qui et al, 2012)} \quad \text{Eq. (6)}$$

As it is understood, considering that each position of the sample has a different grain size and the method utilized by Qui to reach the Eq. (6), the correlation between n and r was found for each sample, as demonstrated in Eq. (7) and (8).

$$n = -0.02 * r + 0.18 \quad (550^{\circ}C \text{ annealed sample}) \quad \text{Eq. (7)}$$

$$n = -0.01 * r + 0.20 \quad (650^{\circ}C \text{ annealed sample}) \quad \text{Eq. (8)}$$

Similarly, equations for the strength coefficient can be derived, as will be described subsequently. Vickers hardness is related to stress, which for most materials, its coefficient of relation is 3 [19]. Also, it is known that stress is proportional to the strength coefficient owing to the power law equation, Eq. (4). Therefore, K is proportional to microhardness, and considering the microhardness distribution for the materials observed in Fig. 5, which is a linear relationship, the equation between K and r can be derived as follow, which are also linear:

$$K = 6.67 * r + 962 \quad (550^{\circ}C \text{ annealed sample}) \quad \text{Eq. (9)}$$

$$K = 3.13 * r + 1043 \quad (650^{\circ}C \text{ annealed sample}) \quad \text{Eq. (10)}$$

Additionally, an average was taken on the Eqs. (7,8) in order to provide a variable to present a single work-hardening exponent for the gradient materials. As the work-hardening exponents of the functionally graded samples are a function of radius, the average work-hardening exponent can be calculated

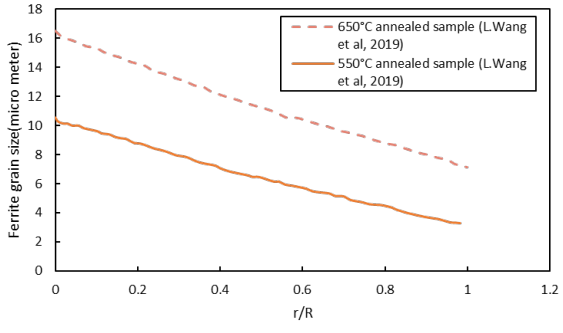

Fig. 4. The ferrite grain size distribution with respect to r/R for samples with 650 °C and 550 °C annealing temperatures. The data for the figure above was extracted from Wang et al. experiment [18].

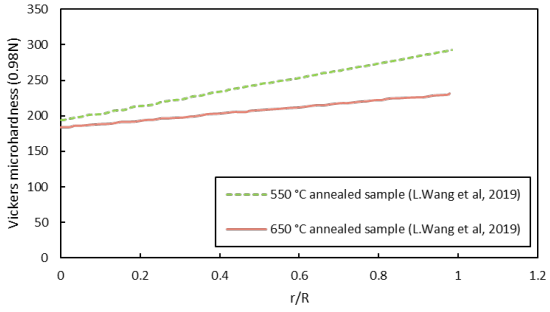

Fig. 5. The Vickers microhardness with respect to r/R for samples with 550 °C and 650 °C annealing temperatures. The data for the figure above was extracted from Wang et al experiment[18].

using Eq. (11).

$$\bar{n} = \frac{\int_A n dA}{A} \qquad \text{Eq. (11)}$$

For each sample after replacing Eqs. (7,8) in the above equation, the average work hardening exponent is calculated as follows:

$$\bar{n} = \frac{\int_0^5 2\pi(-0.02 * r + 0.18)dr}{\pi * 5^2} \qquad \text{Eq. (12)}$$

$$(550^{\circ}\text{C annealed sample})$$

$$\bar{n} = \frac{\int_0^5 2\pi(-0.01 * r + 0.20)dr}{\pi * 5^2} \qquad \text{Eq. (13)}$$

$$(650^{\circ}\text{C annealed sample})$$

For the 550 °C and 650 °C samples, $\bar{n}$ is 0.1095 (0.11) and 0.1657 (0.17), respectively. Ultimately, given the equations of K and n as functions of the position, the procedure can be utilized. Wang's experimental findings are compared to the numerical results.

3. Results and discussion

The numerical method was solved for the functionally graded samples after it was confirmed by the Considère criterion for a homogenous material with theoretical properties. The numerical algorithm was applied with the consideration of the work hardening exponent and strength coefficient equations of the 550 °C and 650 °C annealed functionally graded low carbon steel samples. The results of the numerical computation were graphed alongside the experimental results of the tensile test in Fig. 6 and Fig. 7. When comparing the experimental and numerical results; it can be seen that the algorithm accurately predicts the samples' behavior until the start of necking for the experimental graphs. After necking, the numerical graphs start to deviate from the experimental ones, which is explained subsequently. For a simulation of an ideal case where no imperfections and occurrence of necking are not considered similar to the presented method, in the beginning, work hardening prevails in the competition between the work hardening rate and the reduction rate of the cross-sectional area. However, the hardening rate decreases during the deformation and gradually falls behind the uniform cross-sectional reduction rate. Therefore, the force required to continue the deformation drops, and a peak can be seen. In a case where localization takes place or necking beings, and the samples are made ideally, with no imperfections, necking occurs, and with the start of necking, strain localizes, and the deformation becomes concentrated, resulting in more increase in the reduction rate of the cross-sectional area than before. This is because the rapid rise in the localized area reduction rate will aid the decrease of the work hardening rate in decreasing the load. Therefore, the reduction of force, in this case, will be more rapid than theoretically expected, which is the reason for a very sharp decrease in force after necking in all experimental graphs of engineering stress vs. engineering strain. Moreover, the peak happens much sooner in the experiment due to the possible presence of the geometrical and metallurgical imperfections, as shown in both experimental graphs in Fig. 6 and Fig. 7.

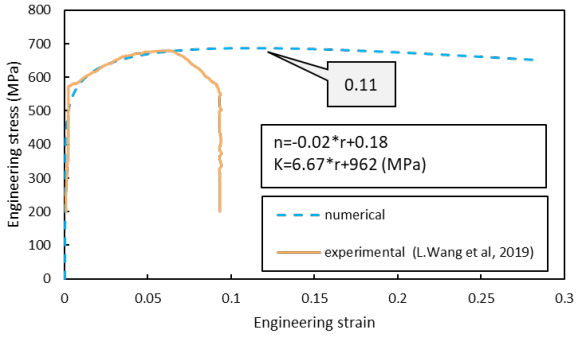

Fig. 6. The calculated engineering stress vs engineering strain for 550 °C annealed sample with $\bar{n} = 0.11$. The experimental data was extracted from [18].

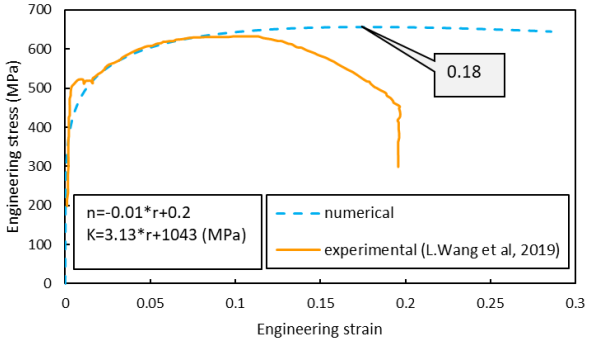

Fig. 7. The calculated engineering stress vs engineering strain for 650 °C annealed sample with $\bar{n} = 0.17$. The experimental result was extracted form [18].

Furthermore, interesting results can be found when comparing the strains at the maximum force in Fig 6 and 7 and the average work hardening exponent, which as calculated above for the 550 °C and 650 °C annealed samples, $\bar{n}$ is 0.1095 and 0.1657 respectively. The true strain at the position where the graphs show a peak for 550 °C and 650 °C annealed samples are 0.1064 and 0.1630, respectively. This demonstrates that the average work-hardening exponent is very close to the ones obtained from the graph, which can be suggested that

the simplest way to predict the instability point for FGM is by making an average of n through its area.

4. Conclusions

The presented algorithm can be a good simulation of the tensile test behavior for the functionally graded low-carbon steels with gradients n and K through the radius of the tensile test samples. From our investigation, it can be concluded that:

- The mathematical algorithm predicts the point of instability of functionally graded material with good agreement with the Considère criterion and can be a good simulation as the diagrams attained from the algorithm showed similar behavior to the ones obtained from the experiment.
- Numerical analysis showed that instability in FGM could be easily predicted based on the calculation of the average strain hardening exponent, which is equal to the true strain at the onset of necking.
- The mathematical analysis showed that even in a case where necking does not occur, the maximum value of force or, in other words, a peak would be seen in the stress-strain graphs because the reduction of the work hardening rate will fall behind the rate of uniform reduction of area.

References

[1] B. Saleh, J. Jiang, A. Ma, D. Song, D. Yang, Effect of main parameters on the mechanical and wear behaviour of functionally graded materials by centrifugal casting: A review, Metals and Materials International. 25 (2019) 1395–1409. https://doi.org/10.1007/s12540-019-00273-8.

[2] R. Fathi, A. Ma, B. Saleh, Q. Xu, J. Jiang, Investigation on mechanical properties and wear performance of functionally graded AZ91-SiCp composites via centrifugal casting, Materials Today Communications. 24 (2020). https://doi.org/10.1016/j.mtcomm.2020.101169.

[3] B. Saleh, J. Jiang, R. Fathi, T. Al-hababi, Q. Xu, L. Wang, D. Song, A. Ma, 30 Years of functionally graded materials: An overview of manufacturing methods, applications and future Challenges, Compos B Eng. 201 (2020). https://doi.org/10.1016/j.compositesb.2020.108376.

[4] Y. Miyamoto, W.A. Kaysser, B.H. Rabin, A. Kawasaki, R.G. Ford, Functionally Graded Materials, first ed., Springer US, New York, NY, 1999. https://doi.org/10.1007/978-1-4615-5301-4.

[5] M. Koizumi, FGM activities in Japan, Composites Part B: Engineering. 28(1997) 1-4. https://doi.org/10.1016/S1359-8368(96)00016-9.

[6] G. Nie, Z. Zhong, Dynamic analysis of multi-directional functionally graded annular plates, Applied Mathematical Modelling. 34 (2010) 608–616. https://doi.org/10.1016/j.apm.2009.06.009.

[7] T.P.D. Rajan, R.M. Pillai, B.C. Pai, Functionally graded Al-Al3Ni in situ intermetallic composites: Fabrication and microstructural characterization, Journal of Alloys and Compounds. 453 (2008). https://doi.org/10.1016/j.jallcom.2006.11.181.

[8] E. Efraim, Accurate formula for determination of natural frequencies of FGM plates basing on frequencies of isotropic plates, Procedia Engineering. 10 (2011) 242–247. https://doi.org/10.1016/j.proeng.2011.04.043.

[9] M. Naebe, K. Shirvanimoghaddam, Functionally graded materials: A review of fabrication and properties, Applied Materials Today. 5 (2016) 223–245. https://doi.org/10.1016/j.apmt.2016.10.001.

[10] S. Kumar Bohidar, R. Sharma, R. Mishra, Functionally graded materials: A critical review, International Journal of Research (IJR). 1 (2014).

[11] M. Sam, R. Jojith, N. Radhika, Progression in manufacturing of functionally graded materials and impact of thermal treatment—A critical review, Journal of Manufacturing Processes. 68 (2021) 1339–1377. https://doi.org/10.1016/j.jmapro.2021.06.062.

[12] R.S. Parihar, S.G. Setti, R.K. Sahu, Recent advances in the manufacturing processes of functionally graded materials: A review, Science and Engineering of Composite Materials. 25 (2018) 309–336. https://doi.org/10.1515/secm-2015-0395.

[13] C.H. Xu, G.Y. Wu, G.C. Xiao, B. Fang, Al2O3/(W,Ti)C/CaF2 multi-component graded self-lubricating ceramic cutting tool material, International Journal of Refractory Metals and Hard Materials. 45 (2014) 125–129. https://doi.org/10.1016/j.ijrmhm.2014.04.006.

[14] P.I. Ichim, X. Hu, J.J. Bazen, W. Yi, Design optimization of a radial functionally graded dental implant, Journal of Biomedical Materials Research Part B: Applied Biomaterials. 104 (2016) 58–66. https://doi.org/10.1002/jbm.b.33345.

[15] P.S. Ghatage, V.R. Kar, P.E. Sudhagar, On the numerical modelling and analysis of multi-directional functionally graded composite structures: A review, Composite Structures. 236 (2020). https://doi.org/10.1016/j.compstruct.2019.111837.

[16] H. Qiu, L.N. Wang, T. Hanamura, S. Torizuka, Prediction of the work-hardening exponent for ultrafine-grained steels, Materials Science and Engineering A. 536 (2012) 269–272. https://doi.org/10.1016/j.msea.2011.11.064.

[17] C.W. Sinclair, W.J. Poole, Y. Bréchet, A model for the grain size dependent work hardening of copper, Scripta Materialia. 55 (2006) 739–742. https://doi.org/10.1016/j.scriptamat.2006.05.018.

[18] L. Wang, B. Li, Y. Shi, G. Huang, W. Song, S. Li, Optimizing mechanical properties of gradi-

ent-structured low-carbon steel by manipulating grain size distribution, Materials Science and Engineering A. 743 (2019) 309–313. https://doi.org/10.1016/j.msea.2018.11.042.
[19] W. F. Hosford, R. M. Caddell, Metal Forming Mechanics and Metallurgy, fourth ed., Cambridge University Press, New York, NY, 2011.
[20] C. V. Nielsen, P.A.F. Martins, Metal Forming: Formability, Simulation, and Tool Design, Elsevier, London, 2021. https://doi.org/10.1016/C2020-0-02428-X.